Review

Magnetic circular dichroism spectroscopy of weakly exchange coupled transition metal dimers: A model study

Stergios Piligkos [a,b], Leonardo D. Slep [a,c], Thomas Weyhermüller [a], Phalguni Chaudhuri [a], Eckhard Bill [a], Frank Neese [a,d,*]

[a] Max-Planck-Institut für Bioanorganische Chemie, Stiftstrasse 34-36, D-45470 Mülheim an der Ruhr, Germany
[b] Department of Chemistry, University of Copenhagen, Universitetsparken 5, DK-2100 Copenhagen, Denmark
[c] Departamento de Quimica Inorganica, Analitica y Quimica Fisica, INQUIMAE, Facultad de Ciencias Exactas y Naturales Universidad de Buenos Aires, Pabellon 2, Ciudad Universitaria, C1428EHA Buenos Aires, Argentina
[d] Universität Bonn, Institut für Physikalische und Theoretische Chemie, Wegelerstr. 12, D-53115 Bonn, Germany

Contents

A R T I C L E   I N F O

A B S T R A C T

A detailed study of the magnetic circular dichroism (MCD) spectra of weakly exchange coupled transition metal heterodimers is reported. The systems consist of three isostructural complexes of the type $[LM(III)(PyA)_3M(II)](ClO_4)_2$ where L represents 1,4,7-trimethyl-1,4,7-triazacyclononanane and PyA^- is the monoanion of pyridine-2-aldoxime. The trivalent metal ion M(III) is either diamagnetic Ga(III) or paramagnetic Cr(III) ($S_{Cr} = 3/2$). The divalent metal ion M(II) is either diamagnetic Zn(II) or paramagnetic Ni(II) ($S_{Ni} = 1$). The three systems **1** (CrZn), **2** (GaNi) and **3** (CrNi) have been structurally and magnetically characterized through magnetic susceptibility measurements. For **1** the zero-field splitting is $D = 0.6\,\text{cm}^{-1}$ while for **2** the value $D = 3.5\,\text{cm}^{-1}$ was found. These values have been fixed in analyzing **3** which was found to be characterized by an antiferromagnetic interaction of $J_{CrNi} = -8.4\,\text{cm}^{-1}$ ($H = -2JS_AS_B$). These values served as benchmarks in the MCD analysis. The zero-field splitting of **1** and **2** was qualitatively recovered using a multi-wavelength analysis of the variable-temperature variable-field (VTVH) MCD data. The observed ligand field bands were assigned to individual d^3 and d^8 multiplets. Using an extension of an earlier developed theory of the nonlinear MCD response, the stunningly complex multiwavelength VTVH-MCD curves of **3** could be quantitatively reproduced with only the relative transition polarizations as input into the fitting procedure. Interestingly, the MCD bands of the minority spin Ni(II) ligand field bands were observed to change sign relative to the parent complex **2**. This behavior has been analyzed. The present work hence provides a benchmark study for the application of MCD spectroscopy to weakly interacting transition metal dimers.

© 2008 Elsevier B.V. All rights reserved.

* Corresponding author at: Universität Bonn, Institut für Physikalische und Theoretische Chemie, Wegelerstr. 12, D-53115 Bonn, Germany.
Tel.: +49 228 73 2351; fax: +49 228 73 9064.
E-mail address: neese@thch.uni-bonn.de (F. Neese).

1. Introduction

Transition metal cages are molecules of great fundamental and technological importance since they display exciting chemical, physical and biological properties. These properties range from catalysis, through molecular magnetism, to the biological function of metalloproteins and metalloenzymes [1]. For this reason, during the last decades, an intense interdisciplinary effort involving chemists, biochemists and physicists has been developed with the purpose to understand the fundamental principles that determine the properties of these compounds. This understanding can only be achieved by establishing the relationship, at the molecular level, between geometric and electronic structure and manifested properties. To this end, the use of spectroscopic techniques of local character is needed, meaning sensitive both to the chemical nature and the geometry of the environment of the metal centre.

The interpretation of the spectroscopic data reflecting the magnetic properties of paramagnetic coordination complexes is most usually performed at a phenomenological level, within the framework of the spin-Hamiltonian formalism [2]. The spectroscopic techniques most commonly used for the determination of the spin-Hamiltonian parameters of the spin states of polymetallic exchange coupled systems are electron paramagnetic resonance (EPR) [3] and inelastic neutron scattering (INS) [4]. These techniques have proven very successful for providing detailed experimental information on the ground and excited spin states of numerous paramagnetic systems. However, their applicability is not universal, as is the case with any other spectroscopic technique, because of intrinsic limitations related to the experimental conditions of measurement. EPR spectrometers employ excitation frequencies roughly up to 700 GHz [5]. Consequently, EPR can be used for the study of systems characterized by maximal anisotropy splitting of the order of $20\,cm^{-1}$. In addition, fast spin-relaxation can lead to a considerable broadening of the detected EPR resonances. In the case of INS measurements, synthesis of relatively large amounts of per-deuterated samples is very often necessary in order to minimize the incoherent scattering from the proton nuclei.

Magnetic circular dichroism (MCD) [6] is a spectroscopic technique that is not limited by the above described limitations. In addition, MCD measurements can be routinely performed in solid state as well as in solution. Another advantage of MCD is that the technique is specific to the chemical nature of the constitutive single-ion centers of a polymetallic system, provided that different types of atoms do not present absorptions in the same spectroscopic region. This offers the possibility to study the magnetic behavior of a given type of paramagnetic centre within a polymetallic system. MCD has been shown to be a powerful method for the study of the ground and excited spin states of polymetallic exchange coupled systems [7] and in particular of SMMs [8].

However, while the formalism for the analysis of individual thermally isolated spin multiplets is reasonably well understood [9,10], it is less clear how to treat exchange coupled systems in which more than one multiplet is thermally accessible. In most previous studies, problems of data interpretation have been circumvented by working in the linear region of the MCD response and only studying the variation of the signal with temperature [11]. In this paper a theoretical approach to the nonlinear MCD behavior of weakly exchange coupled dimers, where several multiplets are thermally populated, is described. Studies on an isostructural series of structurally and magnetically well characterized molecules allow us to show the validity of the formalism that has been used for some years for the analysis of the MCD spectra of exchange coupled dimers. The validation of our model is performed through an experimental study combining MCD and magnetic susceptibility measurements. The theory is based on our earlier formulation of a general MCD theory

[9], that most recently has also been implemented into a rigorous multi-reference configuration interaction (MR-CI) framework [12] as an extension of a much older semi-empirical spin–orbit coupled configuration-interaction approach to MCD [13]. Note also recent works on density functional theory for MCD spectroscopy that is mainly applicable to A- and B-terms [14]. However, in the present work the emphasis is not on the calculation of MCD C-term signs but on the analysis of the nonlinear magnetization behavior.

This formulation of Ref. [9] drastically reduces the number of free parameters required for the interpretation of MCD saturation curves. It is based on an explicit treatment of spin–orbit coupling and the description of the magnetic ground state sublevels by a spin-Hamiltonian model. So far the theory has been applied to metalloproteins and model complexes in various research groups [15]. It is generally successful in reproducing complicated saturation curves and gives access to the polarizations of the electronic transitions relative to the principal axis system of the magnetic coupling tensors. After referencing these polarizations to a molecular axis system detailed insight into the properties of particular metal–ligand bonds is obtained.

2. Results and analysis

2.1. The studied complexes

In the present work, we have studied the nonlinear MCD behavior of weakly exchange coupled dinuclear complexes. The specific aim is the interpretation of the spectroscopic and thermodynamic data obtained on a series of three isostructural complexes of the general formula $[LM(III)(PyA)_3M(II)](ClO_4)_2$, where L represents 1,4,7-trimethyl-1,4,7-triazacyclononane and PyA^- is the monoanion of pyridine-2-aldoxime. Here and for the rest of this study we refer to the dinuclear complex containing a Cr(III) and a Zn(II) center as complex **1**. Complex **2** contains a Ga(III) and a Ni(II) center while complex **3** contains a Cr(III) and a Ni(II) center. The synthesis of complexes **1** and **3** has previously been reported [16]. For the purpose of this study we have synthesized complex **2** by adapting the previously reported experimental protocol for the synthesis of complexes **1** and **3**. The synthetic and spectroscopic details are provided in the supporting information to this paper.

A brief description of the structural parameters of complexes **1**–**3** is given here to discuss the structural characteristics of the studied complexes relevant to this study. The metal core and first coordination sphere of complexes **1**–**3** is illustrated in Fig. 1, in the example of complex **3**. Complexes **1** and **2** have very similar molecular structures. The heterodinuclear complexes **1**–**3** are formed by two distorted octahedra, centered on each of the metal centers, joined by three oximato N–O groups. The first coordination sphere of the M(III) site is formed by three nitrogen atoms from the facially coordinated tridentate macrocyclic amine L and three oxygen atoms from the bridging oximate groups.

The coordination environment of the M(III) site can be described as a trigonally distorted octahedron, the trigonal axis direction being defined by the line running through the center of the two triangular faces defined by the three nitrogen and the three oxygen atoms. The angle formed by the center of the face defined by the three nitrogen atoms, the M(III) site, and the center of the face defined by the three oxygen atoms is of the order of 179°. The two triangular faces are rotated relative to each other by about 60° leading to a distorted octahedral geometry rather than a trigonal prismatic one. The trigonal distortion of the coordination sphere of the M(III) site can be described as a trigonal elongation with respect to the nitrogen atoms of the macrocyclic ligand L, as indicated by angles smaller than 54.74° (of the order of 50°)
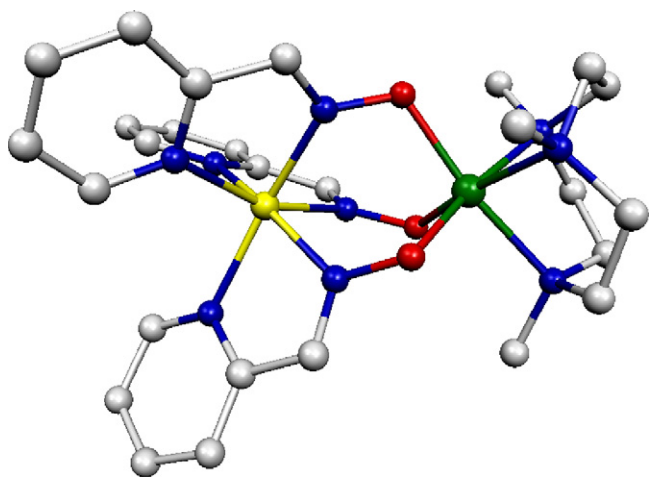
Fig. 1. Molecular structure of complex **3**. Color code: Cr (green), Ni (yellow), nitrogen (blue), oxygen (red), carbon (grey). Hydrogen atoms have been omitted for clarity. (For interpretation of the references to color in this figure legend, the reader is referred to the web version of the article.)

Fig. 2. Molar magnetic susceptibility, $\chi_{M,1}$ (left scale) and effective magnetic moment, $\mu_{eff,1}$ (right scale) of complex **1** in the temperature range from 2 to 290 K and in a field of 1 T.

formed by the previously defined trigonal axis, the M(III) site and each of the three nitrogen atoms of the coordination sphere. With respect to the triangular face defined by the three oxygen atoms of the oximato groups a trigonal compression is observed as indicated by angles larger than 54.74° (in the range from 57° to 61°) formed by the trigonal axis, the M(III) center, and the three oxygen atoms.

The coordination environment of the M(II) site can also be described as a trigonally distorted octahedron, the trigonal axis direction being defined by the centers of the two triangular faces formed by the three nitrogen atoms of the oximato groups and by the three nitrogen atoms of the pyridine groups, all six nitrogen atoms being provided by the pyridine-2-aldoxime ligand. The angle formed by the center of the face defined by the three nitrogen atoms of the oximato groups, the M(II) site, and the center of the face defined by the three nitrogen atoms of the pyridine groups is again of the order of 179°. The two triangular faces are rotated relative to each other by about 29° for **1**, 38° for **2**, and 37° for **3**, leading to an intermediate distortion between octahedral and trigonal prismatic. A trigonal elongation is observed from the triangular face formed by the nitrogen atoms of the oximato groups as indicated by angles in the range 50–53° formed by the previously defined trigonal axis, the M(II) site and the three previously specified nitrogen atoms. A trigonal compression is observed from the side of the triangular face formed by the three nitrogen atoms of the pyridine groups as indicated by angles in the range from 57° to 59° formed by the trigonal axis, the M(II) site and the three nitrogen atoms of the pyridine groups.

Finally taking into account that the trigonal axis direction of the M(III) and M(II) coordination polyhedra are misaligned by an angle of the order of 4°, we neglect this small misalignment and consider that the heterodinuclear complex displays a unique trigonal axis the direction of which is defined by the two metal sites. Thus, for the rest of this study we consider that the heterodinuclear complexes **1–3** are characterized by C_3 symmetry, the C_3 axis containing the heterometallic distance vector.

2.2. Magnetic susceptibility

Magnetic susceptibility data of polycrystalline samples of complexes **1–3** were collected in the temperature range 2–290 K in an applied magnetic field of 1 T. In Fig. 2 are shown the molar mag-
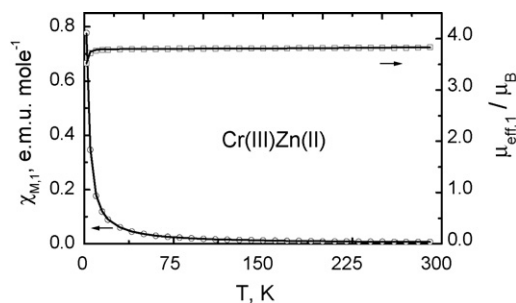
netic susceptibility, $\chi_{M,1}$ and effective magnetic moment, $\mu_{eff,1}$, of complex **1** in the temperature range from 2 to 290 K.

At 290 K $\mu_{eff,1}$ has a value of 3.83 μ_B, indicative of an $S = 3/2$ effective ground spin state. The spin-only value of μ_{eff} for Cr(III) is 3.87 μ_B, for a g-value of 2. Given that Zn(II) is diamagnetic, the magnetic properties of complex **1** are solely determined by the paramagnetic Cr(III) ion. In the temperature range from 290 to 20 K the effective magnetic moment of **1** is essentially temperature independent. At temperatures lower than 20 K $\mu_{eff,1}$ diminishes reaching a value of 3.52 μ_B at 2 K.

The magnetic susceptibility and effective magnetic moment of **1** were modeled by use of spin-Hamiltonian (1)

$$\hat{H}_S = \mu_B B \mathbf{g}_S \hat{\mathbf{S}} + D_S[\hat{\mathbf{S}}_Z^2 - S(S+1)/3] + E_S(\hat{\mathbf{S}}_X^2 - \hat{\mathbf{S}}_Y^2) \qquad (1)$$

that describes the magnetic behavior of a given spin state S of the system. In spin-Hamiltonian (1) μ_B is the electron Bohr magneton, **B** is the magnetic flux density, $\mathbf{g}_S$ is the g-matrix, D_S is the uniaxial anisotropy parameter, and E_S is the rhombic anisotropy parameter of spin state S and $\hat{\mathbf{S}}$ denotes a spin operator. Complex **1** being considered a magnetically mononuclear complex, the spin-Hamiltonian parameters entering spin-Hamiltonian (1) can be considered as the spin-Hamiltonian parameters of the Cr(III) single-ion site. The experimental magnetic data were numerically fitted to spin-Hamiltonian (1) using a least squares fitting routine combined with a full-matrix diagonalization algorithm. The best-fit spin-Hamiltonian parameters of **1** obtained are an isotropic g-value, $g_{Cr} = 1.98$, and a uniaxial anisotropy parameter, $D_{Cr} = 0.6$ cm^{-1}, and a vanishing rhombic anisotropy parameter, E_{Cr}, in accordance with the trigonal symmetry of the Cr(III) site. A model of $\mathbf{g}_{Cr}$ less symmetric than isotropic was not necessary to obtain the best-fit of the experimental data to spin-Hamiltonian (1).

In Fig. 3 are shown the molar magnetic susceptibility, $\chi_{M,2}$ and effective magnetic moment, $\mu_{eff,2}$, of complex **2** in the temperature range from 2 to 290 K. At 290 K $\mu_{eff,2}$ has a value of 3.01 μ_B,
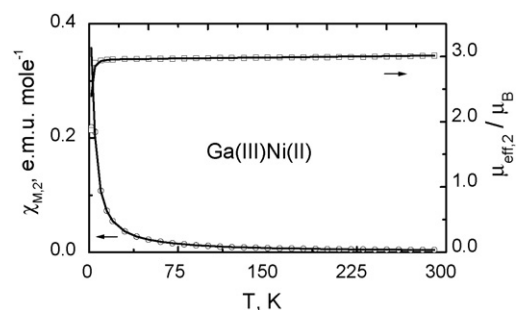

Fig. 3. Molar magnetic susceptibility, $\chi_{M,2}$ (left scale) and effective magnetic moment, $\mu_{eff,2}$ (right scale) of complex **2** in the temperature range from 2 to 290 K and in a field of 1 T.
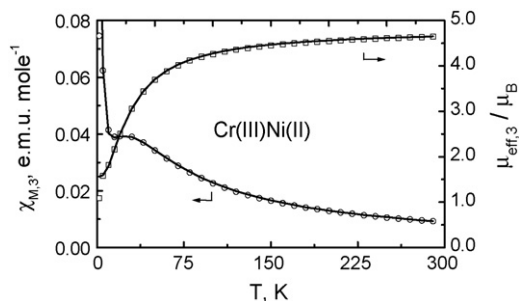
Fig. 4. Molar magnetic susceptibility, $\chi_{M,3}$ (left scale) and effective magnetic moment, $\mu_{eff,3}$ (right scale) of complex **3** in the temperature range from 2 to 290 K and in a field of 1 T.

indicative of an $S = 1$ effective ground spin state. The spin-only value of μ_{eff} for Ni(II) is 2.83 μ_B, for a g-value of 2. Given that Ga(III) is diamagnetic, the magnetic properties of complex **2** are solely determined by the paramagnetic Ni(II) ion. In the temperature range from 290 to 20 K the effective magnetic moment of **2** is essentially temperature independent. At temperatures lower than 20 K $\mu_{eff,2}$ diminishes reaching a value of 2.39 μ_B at 2 K. The magnetic susceptibility and effective magnetic moment of **2** were modeled by use of spin-Hamiltonian (1) as previously described in the case of complex **1**. The obtained best-fit spin-Hamiltonian parameters of **2** are an isotropic g-value, $g_{Ni} = 2.13$, and a uniaxial anisotropy parameter, $D_{Cr} = 3.0$ cm^{-1}. The rhombic anisotropy parameter, E_{Cr}, is zero in accordance with the trigonal symmetry of the Ni(II) site. Again a model of $\mathbf{g}_{Ni}$ less symmetric than isotropic was not necessary to obtain the best-fit of the experimental data to spin-Hamiltonian (1).

In Fig. 4 are shown the molar magnetic susceptibility, $\chi_{M,3}$ and effective magnetic moment, $\mu_{eff,3}$, of complex **3** in the temperature range from 2 to 290 K. The effective magnetic moment of **3** decreases monotonically with decreasing temperature and reaches a value of 1.56 μ_B at 2 K. The $\chi_{M,3}T$ product follows the same temperature dependence decreasing from a value of 2.70 cm^3 K mol^{-1} at 290 K to 0.31 cm^3 K mol^{-1} at 2 K. This behavior is characteristic of an antiferromagnetic interaction between the Cr(III) and Ni(II) centers.

The magnetic susceptibility and effective magnetic moment of **3** were modeled by use of spin-Hamiltonian (2)

$$\hat{H}_{CrNi} = -2\hat{\mathbf{S}}_{Cr}J_{CrNi}\hat{\mathbf{S}}_{Ni}$$

$$+ \sum_{i=Cr,Ni}\left\{\mu_B\mathbf{B}\mathbf{g}_i\hat{\mathbf{S}}_i + \hat{\mathbf{S}}_i\begin{pmatrix} -\frac{1}{3}D_i+E_i & 0 & 0 \\ 0 & -\frac{1}{3}D_i-E_i & 0 \\ 0 & 0 & \frac{2}{3}D_i \end{pmatrix}\hat{\mathbf{S}}_i\right\} \quad (2)$$

where $\hat{S}_{Cr}$ and $\hat{S}_{Ni}$ are spin vector-operators of the paramagnetic Cr(III) and Ni(II) sites, respectively, and J_{CrNi} is the isotropic exchange parameter between the Cr(III) and Ni(II) centers. For the numerical fitting of the temperature dependence of the magnetic susceptibility and effective magnetic moment of **3** we have used the g-values and uniaxial anisotropy parameters determined by the previously described analysis of complexes **1** and **2**. In this way only one free parameter is included in spin-Hamiltonian (2), namely, the isotropic exchange parameter between the Cr(III) and Ni(II) centers. The best-fit value was $J_{CrNi} = -8.4$ cm^{-1}.

2.3. Absorption and MCD spectra. Spectroscopic assignments

The electronic absorption spectra of complexes **1–3** are shown in Fig. 5. The high-energy spectroscopic region of these spectra is dominated by intense intraligand π to π^* transitions as indi-
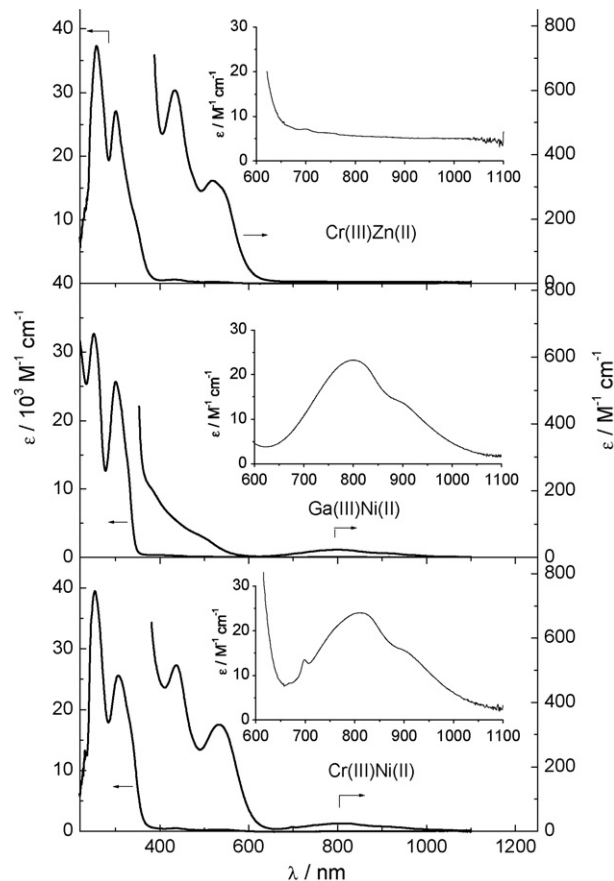

Fig. 5. Room temperature electronic absorption spectra of complexes **1** (top), **2** (middle), and **3** (bottom). The extinction coefficients of the d–d transitions observed in complexes **1–3** are reported in the scale on the left hand-side. The inset shows the intensity in the 600–1100 nm spectroscopic region.

cated by the large molar extinction coefficients of the order of 10^4 M^{-1} cm^{-1}. Complex **1** displays two absorptions centered at about 435 and 528 nm and no absorption at the 650–1100 nm spectroscopic region except a sharp weak band centered at around 700 nm. Complex **2** presents two broad unsymmetrical bands in the regions 370–570 nm and 650–1100 nm. The absorption spectrum of complex **3** can be described as a superposition of the absorption spectra of complexes **1** and **2**. This is nicely illustrated in the spectroscopic region 650–1100 nm of the absorption spectrum of complex **3** where to the broad unsymmetrical band originating from the absorption of the Ni(II) center is superimposed a sharp weaker resonance, centered at 700 nm, originating from the absorption of the Cr(III) centre. It is of interest to mention here that the linewidth of the absorption spectrum of complex **3** is of the same order of magnitude as the linewidth of the absorption spectra of complexes **1** and **2**. This indicates that no prominent pair excitations are taking place in complex **3**.

For complex **1** the two bands observed at 435 and 528 nm are characterized by molar extinction coefficients of 640 and 270 M^{-1} cm^{-1}, respectively. They are attributed to the $^4A_2$ to $^4T_1$ and the $^4A_2$ to $^4T_2$ spin-allowed d–d transitions, respectively, of the Cr(III) ion in octahedral symmetry [17]. However, as it has been discussed in previous sections, the Cr(III) center in **1** is trigonally distorted and is characterized by C_3 rather than octahedral symmetry. In this case one would expect each of the previously identified transitions to split in two bands as consequence of the symmetry lowering.
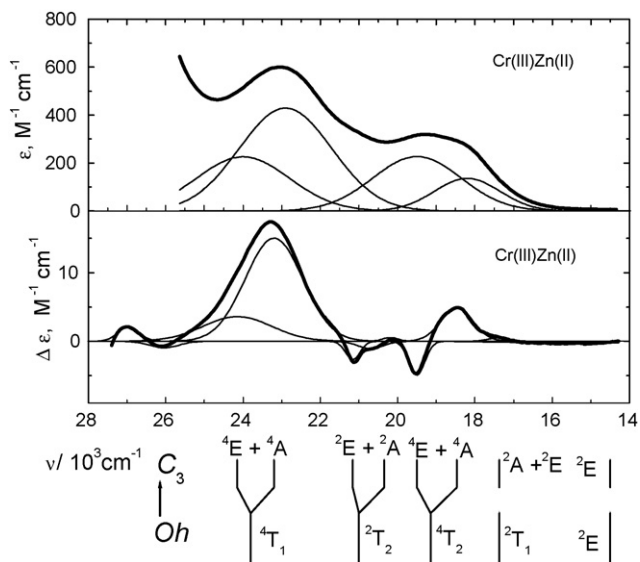
Fig. 6. Simultaneous Gaussian deconvolution of the 28,000–14,000 cm^{-1} spectroscopic region of the room temperature electronic absorption spectrum of **1** and of the MCD spectrum of a frozen solution of **1** in butyronitrile recorded at 5 K in a magnetic field of 3 T.

Fig. 7. Simultaneous Gaussian deconvolution of the 29,000–9000 cm^{-1} spectroscopic region of the room temperature electronic absorption spectrum of **2** and of the MCD spectrum of a frozen solution of **2** in butyronitrile recorded at 5 K in a magnetic field of 3 T.

Fig. 6 shows the simultaneous Gaussian deconvolution of the 28,000–14,000 cm^{-1} spectroscopic region of the room temperature electronic absorption spectrum of **1** and of the MCD spectrum of a frozen solution of **1** in butyronitrile recorded at 5 K in a magnetic field of 3 T. The simultaneous Gaussian deconvolution of the absorption and MCD spectra of **1** reveals that the two previously mentioned spin allowed d–d transitions are indeed split each in two components reflecting the splitting of the orbital triplet electronic T terms of the Cr(III) ion in octahedral symmetry to orbital doublet E and orbital singlet A terms in C_3 symmetry [17]. The ligand field nature of the above described transitions is confirmed by their small C/D ratios, calculated by use of Eq. (3) [6]:

$$\frac{C}{D} = \frac{k_B T}{\mu_B B} \frac{\int \frac{\Delta\varepsilon(\nu)}{\nu} d\nu}{\int \frac{\varepsilon(\nu)}{\nu} d\nu} \tag{3}$$

where k_B is the Boltzmann constant, T is the temperature of the MCD experiment, and $\Delta\varepsilon$ and ε are the observed MCD and absorption intensities at frequency ν. The C/D ratios for the transitions centered at 24,150 and 23,200 cm^{-1} ($^4A_2$ to $^4E(^4T_1)$ and $^4A(^4T_1)$), and for the transitions centered at 19,490 and 18,450 cm^{-1} ($^4A_2$ to $^4E(^4T_2)$ and $^4A(^4T_2)$) are 0.029, 0.054, −0.010, and 0.044, respectively. In addition, the signed nature of the MCD spectrum allows the identification of the spin forbidden $^4A_2$ to $^2T_2$ d–d transition, centered at around 21,000 cm^{-1}, that is also split into E and A components (21,140 and 20,700 cm^{-1}, $^4A_2$ to $^2E(^2T_2)$ and $^4A_2$ to $^2A(^2T_2)$). Finally, the Gaussian deconvolution of the tail of the MCD intensity profile in the spectroscopic region 17,500–14,000 cm^{-1} allows the identifications of the $^4A_2$ to $^2E(^2T_1)$, $^4A_2$ to $^2A(^2T_1)$, and $^4A_2$ to ^2E spin forbidden transitions, as shown in Fig. 6.

For complex **2** the unsymmetrical broad absorption band in the 370–570 nm spectroscopic region of the room temperature absorption spectrum is characterized by molar extinction coefficients in the range 200–100 M^{-1} cm^{-1}. The second unsymmetrical broad absorption band of complex **2**, in the spectroscopic region 650–1100 nm, is characterized by a molar extinction coefficient of about 30 M^{-1} cm^{-1}. This is indicates that ligand field transitions of the Ni(II) complex are observed in the above two spectroscopic regions.
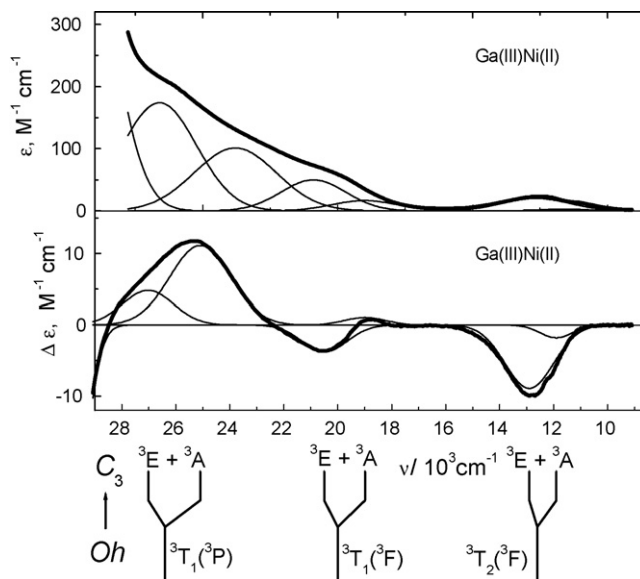
Fig. 7 shows the simultaneous Gaussian deconvolution of the 29,000–9000 cm^{-1} spectroscopic region of the room temperature electronic absorption spectrum of **2** and of the MCD spectrum of a frozen solution of **2** in butyronitrile recorded at 5 K in a magnetic field of 3 T. The simultaneous Gaussian deconvolution of the absorption and MCD spectra of **2** reveals that four individual transitions can be identified for **2** in the spectroscopic region 29,000–17,000 cm^{-1}. These four bands can be attributed to the trigonally split components of the $^3A_2$ to $^3T_1(^3P)$ and $^3A_2$ to $^3T_1(^3F)$ spin-allowed d–d transitions of the Ni(II) ion. The two bands centered at 27,000 and 25,100 cm^{-1} can be attributed to the trigonally split $^3A_2$ to ^3E and ^3A components of the $^3A_2$ to $^3T_1(^3P)$ spin-allowed transition of the Ni(II) ion in C_3 symmetry. The C/D ratio of these bands is 0.047 and 0.202, respectively. The two bands centered at 20,500 and 19,000 cm^{-1} can be attributed to the trigonally split $^3A_2$ to ^3E and ^3A components of the $^3A_2$ to $^3T_1(^3F)$ spin-allowed transition of the Ni(II) ion in C_3 symmetry. The C/D ratios of these bands are −0.131 and 0.100, respectively. Finally, the two bands centered at 12,900 and 11,900 cm^{-1} can be attributed to the trigonally split $^3A_2$ to ^3E and ^3A components of the $^3A_2$ to $^3T_2(^3F)$ spin-allowed transition of the Ni(II) ion in C_3 symmetry. The C/D ratios of these bands are −0.793 and −0.957.

In Fig. 8 is shown the room temperature electronic absorption spectrum of **3** and the MCD spectrum of a frozen solution of **3** in butyronitrile recorded at 5 K in a magnetic field of 3 T, as well as the attribution of the observed bands. Both the electronic absorption and MCD spectra of **3** can be described as a superposition of the corresponding spectra of complexes **1** and **2**. However it is important to note at this point that the broad bands centered at 12,900 and 11,900 cm^{-1} have a negative MCD intensity for complex **2** but a positive MCD intensity in the case of complex **3**. This sign difference of the MCD intensity between complexes **2** and **3** will be justified in later sections.

2.4. VTVH-MCD data of complexes **1** and **2**

The theoretical methodology for the interpretation of the saturation behavior of mononuclear paramagnetic systems was presented some years ago [9]. As previously mentioned the heterodinuclear
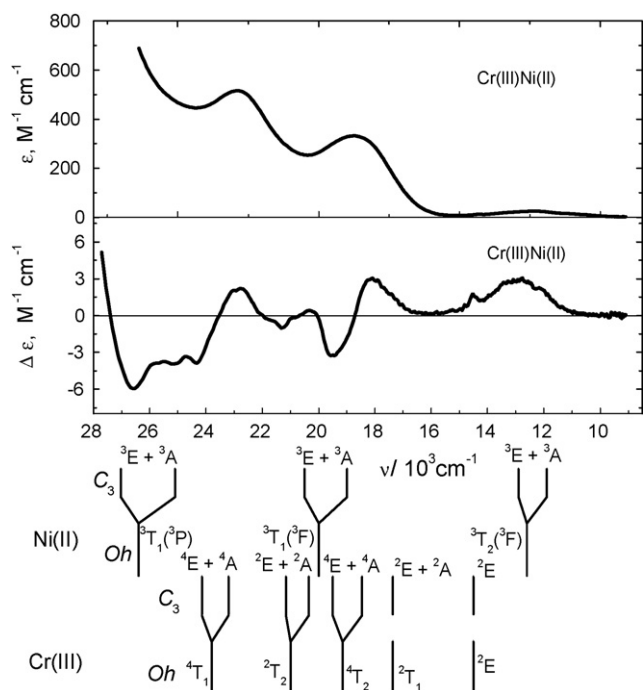
Fig. 8. Simultaneous Gaussian deconvolution of the 28,000–9000 cm^{-1} spectroscopic region of the room temperature electronic absorption spectrum of **3** and of the MCD spectrum of a frozen solution of **3** in butyronitrile recorded at 5 K in a magnetic field of 3 T.

complexes **1** and **2** contain a single paramagnetic center. Consequently, their MCD saturation behavior can be interpreted by use of the previously established model. In the case of randomly oriented samples, the saturation behavior of an MCD transition between spatially nondegenerate states A and J can be modeled in terms of the effective transition moment products, M, between states A and J and the expectation values of the spin operators entering the spin-Hamiltonian describing the paramagnetic ground state, by use of Eq. (4)

$$\frac{\Delta\varepsilon}{E_{AJ}} = \frac{\gamma}{4\pi S} \int_0^\pi \int_0^{2\pi} \sum_i N_i \left(l_x \langle \hat{S}_x \rangle_i M_{yz} + l_y \langle \hat{S}_y \rangle_i M_{zx} \right.$$
$$\left. + l_z \langle \hat{S}_z \rangle_i M_{xy} \right) \sin\theta \, d\theta \, d\phi \qquad (4)$$

where $\Delta\varepsilon$ measures the difference in absorption between left and right circularly polarized light, E_{AJ} is the transition energy, γ is a collection of constants, S is the total spin of the ground state, N_i is the Boltzmann population of the i'th Zeeman sublevel of the paramagnetic ground state, $l_{x,y,z}$ are the direction cosines with respect to the molecular frame of reference (x,y,z), θ and φ are the angles that the projection of the light propagation direction forms with the z and y molecular axes, respectively, M is an effective transition moment product, and $\langle \hat{S}_k \rangle_i \equiv \langle i|\hat{S}_k|i \rangle$ is the expectation values of the k'th component of the spin operator $\hat{S}$ over the ith magnetic eigenstate. These expectation values are obtained by matrix diagonalisation of spin-Hamiltonian (1). Through these spin-expectation values and the Boltzmann populations the spin-Hamiltonian parameters g, D, and E are introduced in the fitting model of the MCD magnetization curves.

VTVH-MCD spectra of a frozen solution of **1** in butyronitrile showed that the detected intensity is strongly temperature and field dependent throughout the investigated spectroscopic region (270–1100 nm). This behavior is termed a C-term behavior. The saturation behavior of the MCD intensity of **1** was monitored at five
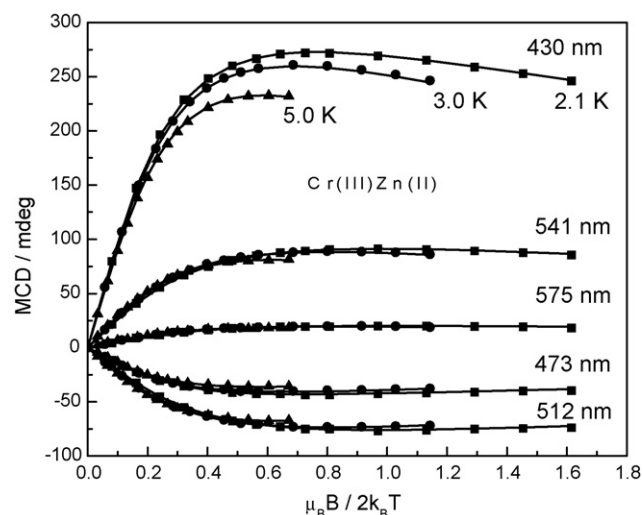

Fig. 9. VTVH-MCD saturation curves of a frozen solution of **1** in butyronitrile in the temperature range 2.1–5 K and in magnetic fields in the range 0–10 T.

different wavelengths, namely, 430, 473, 512, 541, and 575 nm in the temperature range 2.1–5 K and in magnetic fields in the range 0–10 T. The obtained experimental VTVH-MCD data of **1** are shown in Fig. 9. The experimental data at all wavelengths were simultaneously fitted to the model of Eq. (4) by a least square fitting algorithm. For a system containing a single paramagnetic center the fitting of the VTVH-MCD saturation curves involves, at a given wavelength, independent fitting of the relevant spin-Hamiltonian parameters entering spin-Hamiltonian (1), namely, the g-values and the uniaxial and rhombic anisotropy parameters and three effective transition moment products entering Eq. (4). To avoid over-parameterization of the used model it is necessary to constrain some of these parameters. We fixed the g-values to $g_{Cr} = 1.98$, the value obtained by magnetization measurements. In addition a vanishing rhombic parameter, E, was enforced in the fitting procedure in order to take into account the axial symmetry of the Cr(III) center in **1**. Furthermore, for the same reason the effective transitions moment products M_{yz} and M_{zx} were enforced to be equal. These assumptions result in the use of only two free fitting parameters at each wavelength, namely the effective transition moments M_{yz}, M_{zx} and M_{xy} and a common free fitting parameter for all simultaneously fit wavelengths, namely the uniaxial anisotropy parameter D. This simultaneous multi-wavelength fitting approach places severe constraints to the fitting procedure, rendering the obtained results reliable. The trigonal axis of complex **1** is assumed to be the quantization axis. Consequently, the z-component of the uniaxial anisotropy tensor of **1** is collinear to the trigonal axis, as required by symmetry, and to the quantization axis. The best-fit uniaxial anisotropy parameter obtained by modeling the VTVH-MCD data of **1** is $D_{Cr} = 0.60 \pm 0.10$ cm^{-1}. This value is in excellent agreement with the value obtained by the interpretation of the magnetic susceptibility data of **1**. The best-fit effective transition moment products of the observed MCD transitions, obtained by the interpretation of the VTVH-MCD data of **1**, are given in Table 1.

VTVH-MCD spectra of a frozen solution of **2** in butyronitrile also revealed that the detected intensity is strongly temperature and field dependent throughout the investigated spectroscopic region (270–1100 nm). The saturation behavior of the MCD intensity of **2** was monitored at three different wavelengths, namely, 780, 830, and 880 nm in the temperature range 2.1–5 K and in magnetic fields in the range 0–10 T. The obtained experimental VTVH-MCD data of **2** are shown in Fig. 10. Like in the case of complex **1**, the experimen-

Table 1

Best-fit effective transition moment products of the observed MCD transitions obtained by the simultaneous fit of the VTVH-MCD data obtained on a frozen solution of **1** in butyronitrile at five different wavelengths, namely, 430, 473, 512, 541, and 575 nm, in the temperature range 2.1–5 K and in magnetic fields in the range 0–10 T.

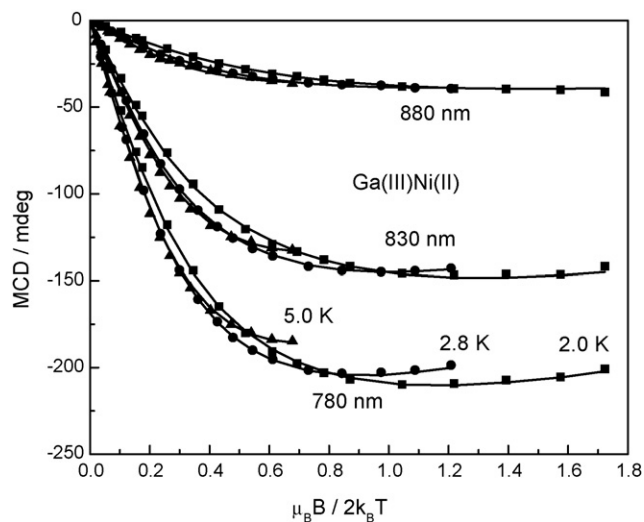| Wavelength (nm)	Cr(III)	
	M_{zx}, M_{yz}	M_{xy}
430	193.0	210.0
473	−100.0	110.0
512	−54.5	−76.0
541	20.5	181.0
575	9.5	30.0

Fig. 10. VTVH-MCD saturation curves of a frozen solution of **2** in butyronitrile in the temperature range 2–5 K and in magnetic fields in the range 0–10 T.

tal data at all three wavelengths were simultaneously fitted to the model of Eq. (4) by a least square fitting algorithm. The same model of orientation of the uniaxial anisotropy tensor of **2** was adopted as in the case of **1**. In addition, as in the case of **1**, an axial model was enforced during the fitting procedure with respect to the values of the rhombic parameter and the effective transition moment products. Having fixed the g-value of Ni(II) to $g_{Ni} = 2.10$, the best-fit uniaxial anisotropy parameter obtained for the Ni(II) center is $D_{Ni} = 3.50 \pm 0.50\,cm^{-1}$. Again this value is in excellent agreement with the value obtained by the interpretation of the magnetic susceptibility data of **2**. The best-fit effective transition moment products obtained by the interpretation of the VTVH-MCD data of **2** are given in Table 2.

The MCD simulations also have a bearing on the sign of the ZFS parameter D. Typically, the simulations are not highly sensitive to this sign but more so than magnetic susceptibility data. This issue

Table 2

Best-fit effective transition moment products of the observed MCD transitions obtained by the simultaneous fit of the VTVH-MCD data obtained on a frozen solution of **2** in butyronitrile at three different wavelengths, namely, 780, 830, and 880 nm, in the temperature range 2–5 K and in magnetic fields in the range 0–10 T.

Wavelength (nm)	Ni(II)	
	M_{zx}, M_{yz}	M_{xy}
780	−166.5	−128.0
830	−94.0	−155.0
880	−28.0	−44.0

is best explored by recording the best-fit error surface as a function of D for both complexes (Fig. 11).

In the case of **2** the error surface confirms unambiguously the magnitude and sign of D. For **1**, the global minimum points to a positive D value although the situation is not as clear cut as with **2**.

A common feature of the VTVH-MCD spectra of complexes **1** and **2** is that the detected intensity at a given wavelength does not change sign throughout the range of temperature and applied magnetic field explored. This sign conservation is characteristic of a C-term behavior originating from a magnetically isolated paramagnetic center. We will see in later sections that an interesting feature of the VTVH-MCD spectra of systems containing magnetically coupled paramagnetic centers is the potential sign reversal of the MCD signal upon temperature and/or applied magnetic field variation.

2.5. Theoretical approach to VTVH-MCD data of interacting dimers

The case we treat is that of an electronic transition in a dimer with weak exchange coupling in the ground *and* the electronically excited state [9]. The dimer is furthermore assumed to be asymmetric, such that the electronic transition is essentially localized on one site. This situation certainly applies to the molecules of this study as well as many others; for example also to the important case of diferrous dimers with different local symmetries around the two ferrous ions [18]. Since under the circumstances of potentially large uniaxial anisotropy compared to the isotropic exchange the total spin S is not a good quantum number, it is most convenient to work in the uncoupled representation. Eq. (6) of Ref. [9] is then modified as follows: to sum over all components of the ground and excited state manifolds that are created by the orbital configurations of the ground state $\left| A S_A M_A S_B M_B \right\rangle$ and the excited state $\left| J_A S_A M_A S_B M_B \right\rangle$ configuration, with J_A being an excitation localized on site A respectively:

$$\frac{\Delta\varepsilon}{E_{AJ}} = -\gamma \sum_{u,v,w} t_{uvw} l_u \sum_i N_i \sum_{M_A,M_B M'_A,M'_B} ImU(M_A M_B \left| i \right)^* U(M'_A M'_B \left| i \right)$$

$$\times \sum_{M''_A,M''_B} \left\langle A S_A M_A S_B M_B \left| m_v \right| J_A S_A M''_A S_B M''_B \right\rangle$$

$$\times \left\langle J_A S_A M''_A S_B M''_B \left| m_w \right| A S_A M'_A S_B M'_B \right\rangle \tag{5}$$

Here, *i* sums over all eigenstates of the spin-Hamiltonian (2), with Boltzmann population N_i and **U** denotes the matrix of expansion coefficients. All other symbols are explained in detail in Ref. [9]. Because the electronically excited states are assumed localized the spin–orbit coupling matrix elements between the ground and the locally excited states can be approximated as [9,19].

$$\left\langle A S_A M_A S_B M_B \left| H_{SOC} \right| J_A S_A M'_A S_B M'_B \right\rangle_0$$

$$\approx \delta_{M_B M'_B} \sum_{m=0,\pm1} (-1)^m Y^{AJ_A}_{-m} \begin{pmatrix} S_A & 1 & S_A \\ M_A & m & M'_A \end{pmatrix} \tag{6}$$

where the subscript zero on the matrix element denotes that it refers to the zero order states that are not corrected for spin–orbit coupling. Here $Y^{AJ_A}_{-m}$ is a reduced matrix element [9,19–22]. Using Eqs. (5) and (6), the derivation of the MCD C-term response is carried through as explained in detail in Ref. [9] and mathematically documented in the supporting information of this reference. The effective equation that is obtained for a transition localized on site A as a function of magnetic coupling parameters and transition
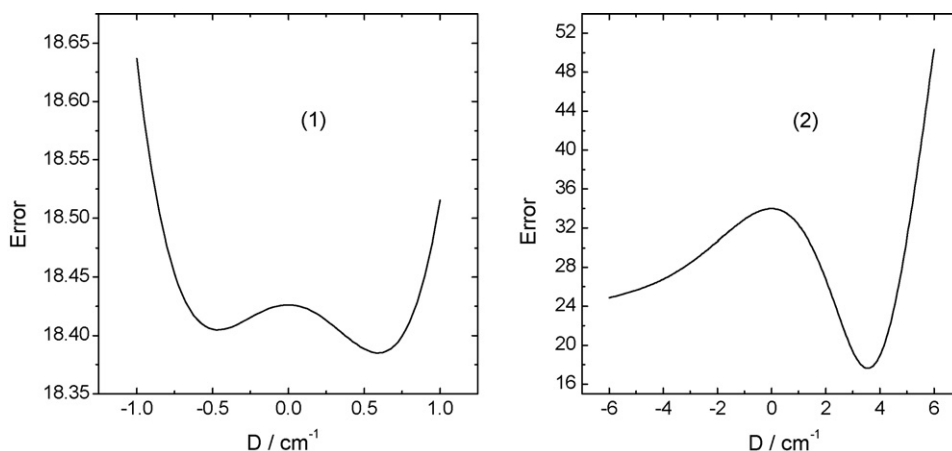
Fig. 11. Least square error surface for 1 (left) and 2 (right) as a function of the zero-field splitting parameter D.

polarizations and averaged over all molecular orientations is [23]

$$\frac{\Delta\varepsilon}{E_{AJ}} = \frac{\gamma}{4\pi S_A} \int_0^\pi \int_0^{2\pi} \sum_i N_i \left(l_x \langle \hat{S}_{A,x} \rangle_i M_{yz} + l_y \langle \hat{S}_{A,y} \rangle_i M_{zx} \right.$$
$$\left. + l_z \langle \hat{S}_{A,z} \rangle_i M_{xy} \right) \sin\theta \, d\theta \, d\phi \qquad (7)$$

Here, the M's are effective transition dipole moment products and $\langle S_{A,p} \rangle_i$ is the p'th component of the spin-expectation value of the i'th ground state sublevel *localized on site A*. Eq. (7) is a particular convenient result because it suggests that for a transition localized on subunit A, the MCD response is simply obtained by extracting the spin-expectation values of the excited subunit from the generally complicated and convoluted ground state eigenfunctions of the coupled dimer. Obviously, an essentially unchanged analysis would apply to systems with more than two magnetic centers as long as one can study an isolated band of an individual center. The only modification is the then the use of a more general spin-Hamiltonian that includes all magnetic centers. Using the spin-Hamiltonian (2) (or a generalization of it), these eigenfunctions can be calculated in a parametric way. Numeric simulations and least squares fits of MCD data to Eq. (7) then yield information about the ground state magnetic coupling parameters and the transition polarizations.

2.6. VTVH analysis of the magnetically interacting system

As in the case of complexes **1** and **2**, VTVH-MCD spectra of a frozen solution of **3** in butyronitrile showed that the detected intensity is strongly temperature and field dependent throughout the investigated spectroscopic region (270–1100 nm). The saturation behavior of the MCD intensity of complex **3** was monitored at five different wavelengths, namely, 438, 514, 552, 768, and 790 nm in the temperature range 2–50 K and in magnetic fields in the range 0–10 T. In analogy to the case of complexes **1** and **2**, the experimental data at all five wavelengths were simultaneously fitted to the model of Eq. (7) by a least square fitting algorithm. The obtained experimental VTVH-MCD data of **3**, at 438, 514, and 768 nm, are shown in Fig. 12. The spin expectation values and Boltzmann populations entering Eq. (7) were calculated by numerical diagonalisation of spin-Hamiltonian (2). Spin-Hamiltonian (2) contains only one free fit parameter, namely the isotropic exchange interaction between the Cr(III) and Ni(II) sites. The rest of the relevant spin-Hamiltonian parameters for the fitting of the VTVH-MCD data of complex **3**, namely, the g-values and uniaxial anisotropy parameters of the Cr(III) and Ni(II) sites, were fixed to the values obtained by the analysis of the VTVH-MCD data of complexes **1** and **2**. The obtained best-fit isotropic exchange parameter between the Cr(III) and the Ni(II) sites is $J_{CrNi} = -6.7 \pm 0.5 \, cm^{-1}$. This value is to be compared to the value $J_{CrNi} = -8.4 \, cm^{-1}$ obtained by analysis of the magnetic susceptibility data of **3**. The best-fit effective
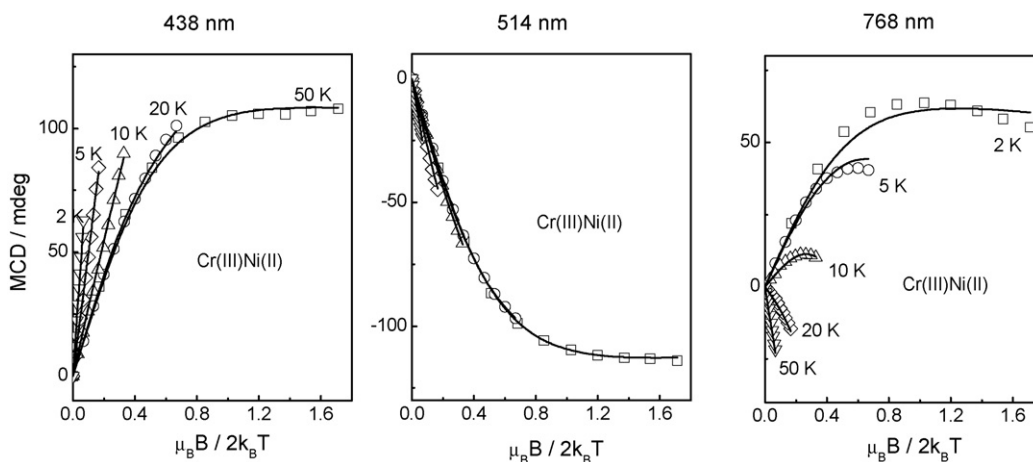

Fig. 12. VTVH-MCD saturation curves of a frozen solution of **3** in butyronitrile in the temperature range 2–50 K and in magnetic fields in the range 0–10 T.

Table 3

Best-fit effective transition moment products of the observed MCD transitions obtained by the simultaneous fit of the VTVH-MCD data obtained on a frozen solution of **3** in butyronitrile at five different wavelengths, namely, 438, 514, 552, 768, and 790 nm, in the temperature range 2–50 K and in magnetic fields in the range 0–10 T.

Wavelength (nm)	Cr(III)		Ni(II)	
	M_{zx}, M_{yz}	M_{xy}	M_{zx}, M_{yz}	M_{xy}
438	−298.0	−36.0	250.0	−269.0
514	−91.0	−167.0	64.5	−51.0
552	−124.0	512.0	−448.5	921.0
768	0.0	0.0	−84.5	−259.0
790	0.0	0.0	−59.0	−318.0

transition moment products obtained by the interpretation of the VTVH-MCD data of **3** are given in Table 3.

As can be seen in Table 3, the VTVH-MCD saturation behavior of the bands at 438, 514, and 552 nm was modeled by considering the bands to be the result of superimposed independent contributions from absorptions centered on both the Cr(III) and Ni(II) sites. On the contrary, the VTVH-MCD saturation behavior of the two bands centered at 768 and 790 nm, was modeled by considering these bands to be pure Ni(II) bands. A striking difference between the saturation behavior of the three bands at 438, 514, and 552 nm and the two bands at 768 and 790 nm, is that the former retain the sign of the detected intensity throughout the investigated range of temperature and applied magnetic field, while the latter present a sign inversion of the detected MCD intensity at high temperatures. As previously mentioned, the band centered at 768 nm can be considered a pure Ni(II) band. From Eq. (7) one can see that for constant effective transition moment products, the sign of the detected MCD intensity depends on a sum of terms involving the spin-expectation values of the eigenvectors describing the thermally populated spin states of the system, the summation being weighted by the Boltzmann population of each of these eigenvectors. In complex **3**, the Cr(III) and Ni(II) sites are coupled by an antiferromagnetic exchange interaction. This means that the ground spin state of complex **3** is an $S = 1/2$ spin state. The other two spin states of the system are an $S = 3/2$ and an $S = 5/2$ lying at 20.1 and 53.6 cm^{-1} above the ground state, respectively, for $J_{CrNi} = -6.7$ cm^{-1}. The spin expectation values of the spin operators of the Cr(III) and Ni(II) sites in **3**, in the case that the magnetic field is oriented parallel or perpendicular to the C_3 axis, are given in Table 4. The expectation values reported in Table 4 have been determined by numerical diagonal-

Table 4

Spin expectation values of the eigenvectors of spin-Hamiltonian (2) for complex **3** calculated with the parameters given in the text and for an external magnetic field strength of 4 T. The $\langle \hat{S}_{x,y} \rangle$ and $\langle \hat{S}_z \rangle$ were calculated with the external field oriented perpendicular or parallel to the C_3 axis, respectively. For the sake of simplicity the eigenvectors of spin-Hamiltonian (2) are labeled by strong exchange limit labels.

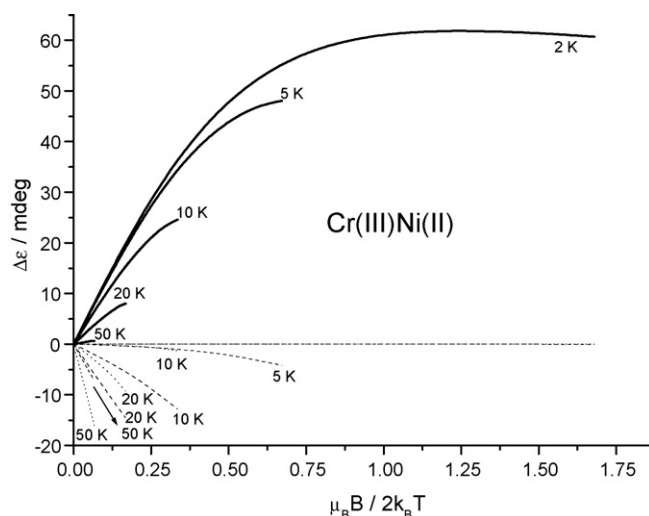| Eigenvector $|S, M_S\rangle$	$\langle \hat{S}_{x,y} \rangle$		$\langle \hat{S}_z \rangle$	
	Cr(III)	Ni(II)	Cr(III)	Ni(II)
$|1/2, -1/2\rangle$	−0.87	0.37	−0.76	0.26
$|1/2, +1/2\rangle$	0.86	−0.37	0.76	−0.26
$|3/2, -3/2\rangle$	−1.05	−0.42	−1.13	−0.37
$|3/2, -1/2\rangle$	−0.31	−0.17	−0.46	−0.04
$|3/2, +1/2\rangle$	0.29	0.18	0.46	0.04
$|3/2, +3/2\rangle$	1.07	0.41	1.13	0.37
$|5/2, -5/2\rangle$	−1.49	−0.99	−1.50	−1.00
$|5/2, -3/2\rangle$	−0.89	−0.57	−0.87	−0.63
$|5/2, -1/2\rangle$	−0.29	−0.18	−0.28	−0.22
$|5/2, +1/2\rangle$	0.30	0.20	0.28	0.22
$|5/2, +3/2\rangle$	0.89	0.56	0.87	0.63
$|5/2, +5/2\rangle$	1.48	0.98	1.50	1.00

Fig. 13. Contributions from the ground and excited spin states of **3** to the 768 nm VTVH-MCD saturation curves of a frozen solution of **3** in butyronitrile in the temperature range 2–50 K and in magnetic fields in the range 0–10 T. The contributions from the $S = 1/2$ ground spin state are represented by a solid line, the contributions from the $S = 3/2$ first excited spin state by a dashed line, and the contributions from the $S = 5/2$ second excited spin state by a dot line.

isation of spin-Hamiltonian (2) with the previously determined best-fit parameters of **3** and for an externally applied magnetic field of 4 T. For the sake of simplicity in Table 4 the various eigenvectors are labeled, within the strong exchange limit, by their total spin S and its projection along the z-axis. From Table 4 one can see that for the ground spin state the spin expectation values on the Ni(II) site have an opposite sign than the projection of the total spin along the z-axis, while for the excited states the spin expectation values on the Ni(II) site have the same sign as the projection of the total spin along the C_3 axis. Because of this behavior the Ni(II) site is termed the minority spin species. The contributions from each of the three spin states of the system to the MCD intensity detected at 768 nm are shown in Fig. 13. In this Figure one observes that the contribution of the ground spin state to the MCD intensity of this band is of positive sign and decreases with increasing temperature, becoming practically negligible at 50 K, as consequence of the progressive equalization of the thermal populations of the Zeeman sublevels with increasing the temperature. On the contrary, the contributions to the MCD intensity of the band at 768 nm from the excited spin states are of negative sign and of increasing intensity with increasing temperature. Thus, the MCD sign and intensity of the band at 768 nm is mainly determined from contributions of the ground spin state at low temperatures and from contributions from the excited spin states at higher temperatures. This sign reversal is associated to the sign reversal of the projected, to the ground and excited spin states, expectation value of $\hat{S}$ for the minority spin species. Thus, monitoring of the VTVH-MCD saturation behavior of the band at 768 nm gives direct access to the spin expectation values of a given center, in this case Ni(II), within a polymetallic system.

3. Discussion

In the present work, we have presented a detailed experimental study of weakly exchange coupled transition metal dimers in an attempt to better understand their magnetic circular dichroism properties. It was shown that three iso-structural dimers of Zn(II)Cr(III) (**1**), Ni(II)Ga(III) (**2**), and Ni(II)Cr(III) (**3**) could be obtained and structurally as well as magnetically characterized

using magnetic susceptibility measurements. Their EPR properties have been reported in Ref. [16]. The absorption and MCD spectra on the ligand field region are well resolved and could be straight-forwardly assigned on the basis of ligand field theory. For the complexes with a single magnetic center it was then shown that the ZFS parameter determined by magnetic susceptibility measurements can be well recovered with MCD spectroscopy using a previously proposed theory of the nonlinear MCD response [9]. Importantly, this theory can be extended to the cases of weakly interacting transition metal dimers. Although this theory has been used for a while [23], it has never been verified in a detailed experimental model study. The present work has been designed to present this validation and unambiguously demonstrates how to extract the exchange coupling parameters for interacting transition metal centers from VTVH-MCD measurements. It is gratifying to see that even the highly complicated, nonlinear MCD magnetization curves, that may even change sign with increasing magnetic field strength or temperature, can be quantitatively reproduced with only a minimal number of fit parameters. Furthermore, we have presented evidence that the sign of the MCD bands provides an experimental means to identify the minority spin species in an exchange-coupled dimer. In the present case, the ligand field bands of the Ni(II) centers changed sign upon going from Ni(II)Ga(III) to Ni(II)Cr(III).

An obvious extension of the theoretical methodology would be to extend the method to symmetric dimers, strongly exchange coupled systems and higher nuclearity clusters. Work along these lines is in progress. The latter extension is particularly important in the framework of large polynuclear transition metal clusters and molecular magnetism. We have already obtained a promising set of MCD data for Cr_8M wheels (M = Zn, Cd, Ni) [24] which could be analyzed with a model highly similar to the one presented here. Classic work on Cr_7M systems was reported by Oganesyan and co-workers [8b].

Taken together we have presented a detailed MCD model study that, we hope, may contribute to a more widespread use of this powerful technique in molecular magnetism. We emphasize that MCD spectroscopy is a sensitive technique with an information content that exceeds that of EPR or magnetic susceptibility techniques. Although MCD has certainly a lower resolution and precision than modern high-field EPR, it is not constrained by relaxation effects and also yields information on excited states and coordination geometries via an analysis of the ligand field region of the spectrum. Unlike susceptibility, MCD is not a bulk measurement and can even be applied to mixtures or only partially pure samples as long as an isolated absorption band for the species of interest can be identified. Owing to recent computational progress exact solutions to giant spin-Hamiltonian eigenvalue problems can now be efficiently obtained which will allow the present methodology to be applied to much larger single-molecule magnets [25]. Studies along these lines are in progress in our laboratories.

Acknowledgements

Appendix A. Supplementary data

Supplementary data associated with this article can be found, in the online version, at doi:10.1016/j.ccr.2008.10.014.

References

[1] (a) R. Sessoli, D. Gatteschi, Angew. Chem. Int. Ed. 42 (2003) 268;
(b) D. Gatteschi, R. Sessoli, J. Villain, Molecular Nanomagnets, Oxford University Press, Oxford, 2006;
(c) G. Christou, D. Gatteschi, D.N. Hendrickson, R. Sessoli, MRS Bull. 25 (2000) 66;
(d) R. Bircher, G. Chaboussant, C. Dobe, H.U. Güdel, S.T. Ochsenbein, A. Sieber, O. Waldmann, Adv. Funct. Mater. 16 (2006) 209;
(e) G. Aromí, E.K. Brechin, Struct. Bond. 122 (2006) 1;
(f) C.J. Milios, S. Piligkos, E.K. Brechin, Dalton Trans. (2008) 1809;
(g) V.L. Pecoraro (Ed.), Manganese Redox Enzymes, VCH Publishers, New York, 1992.
[2] (a) A. Bencini, D. Gatteschi, EPR of Exchange Coupled Systems, Springer-Verlag, Berlin, 1989;
(b) F. Neese, Coord. Chem. Rev. (in press), doi:10.1016/j.ccr.2008.05.014.;
(c) F. Neese, Mag. Res. Biol. (in press).
[3] (a) A. Abragam, B. Bleaney, Electron Paramagnetic Resonance of Transition Ions, Dover, New York, 1986;
(b) F.E. Mabs, D. Collison, Electron Paramagnetic Resonance of d Transition Metal Compounds, Elsevier, Amsterdam, 1992;
(c) D. Gatteschi, A.L. Barra, A. Caneschi, A. Cornia, R. Sessoli, L. Sorace, Coord. Chem. Rev. 250 (2006) 1514.
[4] R. Basler, C. Boskovic, G. Chaboussant, H.U. Güdel, M. Murrie, S.T. Ochsenbein, A. Sieber, ChemPhysChem 4 (2003) 910.
[5] J. Krzystek, A. Ozarowski, J. Telser, Coord. Chem. Rev. 250 (2006) 2308.
[6] (a) S.B. Piepho, P.N. Schatz, Group Theory in Spectroscopy with Applications to Magnetic Circular Dichroism, John Wiley & Sons, New York, 1983;
(b) P.J. Stephens, J. Chem. Phys. 52 (1970) 3489;
(c) P.J. Stephens, Adv. Chem. Phys. 35 (1976) 197;
(d) P.J. Stephens, Ann. Rev. Phys. Chem. 25 (1974) 201;
(e) A.D. Buckingham, P.J. Stephens, Ann. Rev. Phys. Chem. 17 (1966) 399;
(f) E.I. Solomon, E.G. Pavel, K.E. Loeb, C. Campochiaro, Coord. Chem. Rev. (1995) 369.
[7] (a) D. Collison, M. Murrie, V.S. Oganesyan, S. Piligkos, N.R.J. Poolton, G. Rajaraman, G.M. Smith, A.J. Thomson, G.A. Timko, W. Wernsdorfer, R.E.P. Winpenny, E.J.L. McInnes, Inorg. Chem. 42 (2003) 5293;
(b) D. Collison, V.S. Oganesyan, S. Piligkos, A.J. Thomson, R.E.P. Winpenny, E.J.L. McInnes, J. Am. Chem. Soc. 125 (2003) 1168;
(c) J.M. Bradley, A.J. Thomson, E.J.L. McInnes, R.E.P. Winpenny, G. Timco, Dalton Trans. (2008) 3311.
[8] (a) M.R. Cheesman, V.S. Oganesyan, R. Sessoli, D. Gatteschi, A.J. Thomson, Chem. Commun. (1997) 1677;
(b) E.J.L. McInnes, E. Pidcock, V.S. Oganesyan, M.R. Cheesman, A.K. Powell, A.J. Thomson, J. Am. Chem. Soc. 124 (2002) 9219;
(c) N. Domingo, B.E. Williamson, J. Gomez-Segura, P. Gerbier, D. Ruiz-Molina, D.B. Amabilino, J. Veciana, J. Tejada, Phys. Rev. B 69 (2004) 052405;
(d) P. Gerbier, N. Domingo, J. Gomez-Segura, D. Ruiz-Molina, D.B. Amabilino, J. Tejada, B.E. Williamson, J. Veciana, J. Mater. Chem. 14 (2004) 2455.
[9] F. Neese, E.I. Solomon, Inorg. Chem. 38 (1999 1847).
[10] V.S. Oganesyan, S.J. George, M.R. Cheesman, A.J. Thomson, J. Chem. Phys. 110 (1999) 762.
[11] (a) M.R. Cheesman, V.S. Oganesyan, N.J. Watmough, C.S. Butler, A.J. Thomson, J. Am. Chem. Soc. 126 (2004) 4157;
(b) V.S. Oganesyan, M.R. Cheesman, A.J. Thomson, Inorg. Chem. 46 (2007) 10950.
[12] D. Ganyushin, F. Neese, J. Chem. Phys. 128 (2008) 114117.
[13] J.A. Farrar, F. Neese, P. Lappalainen, P.M.H. Kroneck, M. Saraste, W.G. Zumft, A.J. Thomson, J. Am. Chem. Soc. 118 (1996) 11501.
[14] (a) M. Seth, T. Ziegler, J. Chem. Phys. 124 (2006);
(b) M. Seth, T. Ziegler, J. Autschbach, J. Chem. Phys. 122 (2005);
(c) M. Seth, T. Ziegler, A. Banerjee, J. Autschbach, S.J.A. van Gisbergen, E.J. Baerends, J. Chem. Phys. 120 (2004) 10942.
[15] (a) F. Neese, E.I. Solomon, J. Am. Chem. Soc. 120 (1998) 12829;
(b) R. Schenker, M.T. Mock, M.T. Kieber-Emmons, C.G. Riordan, T.C. Brunold, Inorg. Chem. 44 (2005) 3605;
(c) J.L. Craft, B.S. Mandimutsira, K. Fujita, C.G. Riordan, T.C. Brunold, Inorg. Chem. 42 (2003) 859;
(d) T.A. Jackson, J. Xie, E. Yikilmaz, A.-F. Miller, T.C. Brunold, J. Am. Chem. Soc. 124 (2002) 10833;
(e) M.L. Kirk, K. Peariso, Curr. Opin. Chem. Biol. 7 (2003) 220;
(f) K. Ray, A. Begum, T. Weyhermüller, S. Piligkos, J. van Slageren, F. Neese, K. Wieghardt, J. Am. Chem. Soc. 127 (2005) 4403;
(g) E.I. Solomon, M.I. Davis, F. Neese, M.Y.M. Pau, in: J. Telser (Ed.), Paramagnetic Resonance of Metallobiomolecules, Oxford University Press, Oxford, 2003, p. 328;
(g) M.D. Clay, C.A. Cosper, F.E. Jenney, M.W.W. Adams, M.K. Johnson, Proc. Natl. Acad. Sci. U.S.A. 100 (2003) 3796.

[16] S. Ross, T. Weyhermüller, E. Bill, K. Wieghardt, P. Chaudhuri, Inorg. Chem. 40 (2001) 6656.

[17] C.J. Ballhausen, Introduction to Ligand Field Theory, McGraw-Hill, New York, 1962.

[18] (a) P.P. Wei, A.B. Tomter, A.K. Rohr, K.K. Andersson, E.I. Solomon, Biochemistry 45 (2006) 14043;
(b) P.P. Wei, A.J. Skulan, H. Wade, W.F. DeGrado, E.I. Solomon, J. Am. Chem. Soc. 127 (2005) 16098;
(c) K.R. Strand, Y.S. Yang, K.K. Andersson, E.I. Solomon, Biochemistry 42 (2003) 12223;
(d) K.R. Strand, Y.S. Yang, K.K. Andersson, E.I. Solomon, J. Inorg. Biochem. 86 (2001) 445;
(e) S. Pulver, W.A. Froland, B.G. Fox, J.D. Lipscomb, E.I. Solomon, J. Am. Chem. Soc. 115 (1993) 12409;
(f) S. Coates-Pulver, W.H. Thong, J.M. Bollinger, J. Stubbe, E.I. Solomon, J. Am. Chem. Soc. 117 (1995) 12664;

(g) Y.-S. Yang, J.A. Broadwater, B.G. Fox, E.I. Solomon, J. Am. Chem. Soc. 121 (1999) 2770.

[19] F. Neese, E.I. Solomon, Inorg. Chem. 37 (1998) 6568.

[20] F. Neese, E.I. Solomon, in: J.S. Miller, M. Drillon (Eds.), Magnetoscience—From Molecules to Materials, volume IV, Wiley VCH, Weinheim, 2003, p. 345.

[21] D. Ganyushin, F. Neese, J. Chem. Phys. 125 (2006).

[22] F. Neese, T. Petrenko, D. Ganyushin, G. Olbrich, Coord. Chem. Rev. 251 (2007) 288.

[23] E.I. Solomon, T.C. Brunold, M.I. Davis, J.N. Kemsley, S.K. Lee, N. Lehnert, F. Neese, A.J. Skulan, Y.S. Yang, J. Zhou, Chem. Rev. 100 (2000) 235.

[24] O. Cador, D. Gatteschi, R. Sessoli, F.K. Larsen, J. Overgaard, A.-L. Barra, S.J. Teat, G.A. Timco, R.E.P. Winpenny, Angew. Chem. Int. Ed. 43 (2004) 5196.

[25] S. Piligkos, E. Bill, D. Collison, E.J.L. McInnes, G.A. Timco, H. Weihe, R.E.P. Winpenny, F. Neese, J. Am. Chem. Soc. 129 (2007) 760.